

Bulk and Surface Event Identification in p-type Germanium Detectors

L.T. Yang^{a,b}, H.B. Li^{c,*}, L.P. Jia^b, H. Jiang^b, J. Li^b, F.K. Lin^c, S.T. Lin^d,
S.K. Liu^{b,d}, J.L. Ma^a, V. Sharma^c, L. Singh^c, M.K. Singh^c, A.K. Soma^c,
S.W. Yang^c, L. Wang^b, Q. Wang^{a,b,e,f}, H.T. Wong^c, Q. Yue^{b,*}, W. Zhao^b

^a*Department of Physics, Tsinghua University, Beijing 100084*

^b*Key Laboratory of Particle and Radiation Imaging (Ministry of Education) and
Department of Engineering Physics, Tsinghua University, Beijing 100084*

^c*Institute of Physics, Academia Sinica, Taipei 11529*

^d*College of Physical Science and Technology, Sichuan University, Chengdu 610064*

^e*Center for High Energy Physics, Tsinghua University, Beijing 100084*

^f*Collaborative Innovation Center of Quantum Matter, Beijing 100084*

Abstract

The p-type point-contact germanium detectors, due to its sub-keV sensitivities and low internal radioactivity background, are demonstrated to be competitive tools for light dark matter WIMPs searches and may have potential applications in neutrino physics. These detectors exhibit anomalous surface behavior, which has been characterized and dealt with in previous analysis. However, the analysis method rely on spectral shape assumptions and must use external calibration sources. In this report, we purpose an improved method, where in situ data could be used as calibration sources. Data from CDEX-1 and TEXONO experiments will be re-examined and the results are shown to be consistent with both analysis.

Keywords: Dark matter, Radiation detector

1. Introduction

The p-type point-contact germanium detectors ($p\text{Ge}$) have been demonstrated as a potential technique to the rare-event detection experiments, such as the probe of “light” Weakly Interacting Massive Particles (WIMPs) with

*Corresponding author

mass range $1 \text{ GeV} < m_\chi < 10 \text{ GeV}$ and the studies of neutrino-nucleus coherent scattering with reactor neutrinos [1, 2, 3], due to low internal radioactivity background and excellent energy threshold [4]. Note that these features are provided by lithium diffused surface in p-type, not the point-contact.

At the low energy region, the results from China Dark Matter Experiment (CDEX-1) [5, 6, 7] and Kuo-Sheng Neutrino Laboratory Experiment (TEXONO) [8, 9] are inconsistent with those from DAMA [10, 11, 12], CoGeNT [13, 14, 15] and CDMS(Si) [16], which implied the potential positive signatures of WIMPs. This controversial issue generates intense interest and need more experiment results to cross-check.

However, the surface events in $p\text{Ge}$ detectors exhibit anomalous behavior [6, 7, 8, 9, 17, 18, 19], which may lead to false interpretation of the data and limit the sensitivities. The analysis of these anomalous surface events is crucial for experimental challenge and realization of the full potential of this novel detector technique at sub-keV energy.

Quantitative studies on these anomalous surface events are discussed in detail in [9] (denoted as spectral shape method). However, there are several inadequacies with the spectral shape method. In this report, we purpose an improved method (denoted as ratio method), where in situ data will provide important constraints and information in addition to be combined with dedicated calibration data with external sources, to deal with these anomalous surface events.

This report is organized as follows: in Section 2, we introduce the physics of anomalous surface events in $p\text{Ge}$ detectors and summarize previous analysis on spectral shape method. In Section 3 we present the ratio method, which is based on the ratios of count rates, to analysis these anomalous surface events. In Section 4, we manifest the ratio method with data from CDEX-1 [5, 6, 7] and TEXONO [8, 9].

We will use same notations as described in [6, 7, 9] for different types of physics events. AC and CR denote the anti-Compton detector and the cosmic-ray veto system, respectively. The superscript $- (+)$ denotes anti-coincidence (coincidence) with the $p\text{Ge}$ signal, e. g., dark matter candidate data will be AC^- (without anti-Compton(NaI) triggered) in CDEX-1 experiment and $\text{CR}^- \otimes \text{AC}^-$ (without anti-Compton(NaI) triggered and without cosmic-ray induced) in TEXONO experiment.

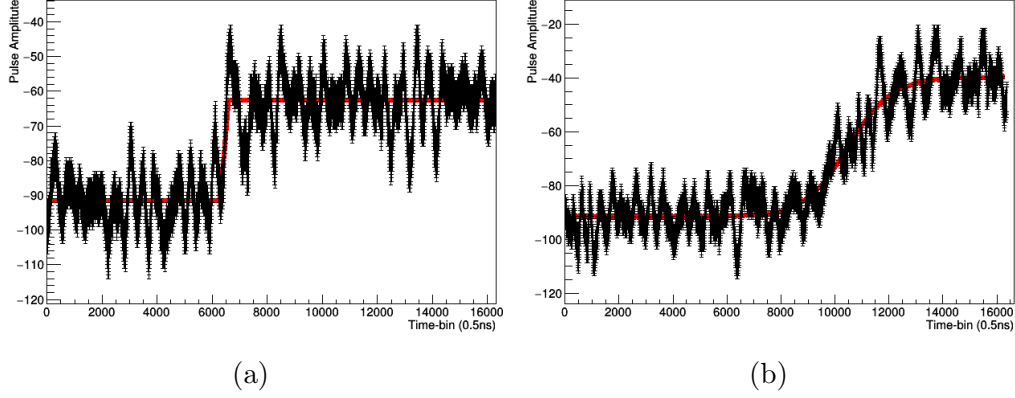


Figure 1: Voltage vs. Time of a typical (a) fast rise-time pulse, 1.8 keV bulk signal and (b) slow rise-time pulse, 2.3 keV surface signal.

2. Anomalous Surface Events in $p\text{Ge}$ Detectors

2.1. Physics

During the ionization process in germanium detector, the current caused by electron-hole pair drifting are recorded. The drift time depends on the location of the ionization, when it occurs at the lithium diffused layer (~ 1 mm) [20] at the surface of the germanium, the drift time will be slower, and only partial charge will be collected [17, 18]. The charge collection efficiency as a function of the depth into the surface has been measured and simulated [21]. We will name these events as “surface”, while those not occur at this diffused layer as “bulk”.

The signals are processed as cumulative charge, a difference of the electron-hole pair drift time will produce signals of different rise-time as shown in Fig. 1, this feature allows us to separate bulk events and surface events.

A hyperbolic tangent function is used to fit the voltage of signals to quantify the rise-time [9]:

$$\frac{1}{2}A_0 \times \tanh\left(\frac{t - t_0}{\tau}\right) + P_0 \quad (1)$$

where A_0 is amplitude of the signal which is proportional to energy, t is time of signal which serves as independent variable, t_0 is timing of the signal rising, in which zero timing is defined by data acquisition trigger, P_0 is voltage offset, and τ is the rise-time.

However, due to electronic noise, bulk events could be falsely identified as surface events (or vice versa), especially at low energy region (<2 keV). These “leakages” have to be dealt with to obtain real bulk or surface count rates.

In this report, we take the same approach as [6, 7, 9] for various events selection before bulk/surface separation, including discard those with extreme slow rise-time ($\tau > 10 \mu s$). Subsequent analysis will show that bulk events leak into extreme slow rise-time region is negligible, thus justifies the events selection. Those counts are then added to the total surface counts at the final surface spectra.

2.2. B/S selection: Spectral Shape Method

We have established a cut-based scheme for bulk/surface (denoted B/S) separation on dark matter results of CDEX-1 and TEXONO experiments [6, 7, 9]. Bulk leakage (denoted by ϵ_{BS}) and surface contamination (denoted by $1 - \lambda_{BS}$) defined by a B/S-cut are used to correct measured bulk (B_m) or surface (S_m) to real bulk (B_r) or surface (S_r) by the coupled equations:

$$\begin{aligned} B_m &= \epsilon_{BS} B_r + (1 - \lambda_{BS}) S_r \\ S_m &= \lambda_{BS} S_r + (1 - \epsilon_{BS}) B_r, \end{aligned} \quad (2)$$

with an additional unitary constrain: $B_m + S_m = B_r + S_r$, solving the Eq. 2 yield:

$$\begin{aligned} B_r &= \frac{\lambda_{BS} B_m - (1 - \lambda_{BS}) S_m}{\epsilon_{BS} + \lambda_{BS} - 1} \\ S_r &= \frac{\epsilon_{BS} S_m - (1 - \epsilon_{BS}) B_m}{\epsilon_{BS} + \lambda_{BS} - 1}. \end{aligned} \quad (3)$$

Since there are two unknown parameters, ϵ_{BS} and λ_{BS} , at least two sources with different bulk to surface ratio are needed to solve Eq. 2. In CDEX-1 experiment, four calibration sources (^{137}Cs , ^{241}Am , ^{57}Co and ^{60}Co) [6, 7] are used. The measured spectra of these sources are calibrated to their estimated bulk spectra (B_r) from GEANT4 simulation to solve ϵ_{BS} , λ_{BS} . The target sample, i. e., dark matter candidate data and ambient gamma background are then corrected by ϵ_{BS} and λ_{BS} . Due to the nature of this method, we will name it spectral shape method in this report.

However, there are several disadvantages with the spectral shape method:

(1) **Spectral shape assumption.**

Only sources with known spectral shape from simulations could be used as calibration sources, that does not include in situ data, e. g., dark matter candidate and ambient gamma background, which might pose a problem in long term data taking, where data of external calibration sources have to be retaken from time to time to synchronize with in situ data.

In CDEX-1 and TEXONO procedure [6, 7, 9], the flat spectral shape of B_r of calibration sources are evaluated from GEANT4 simulation package, which depends on the detector structure and physics process subroutine used in the simulation. The ambient gamma and cosmic induced events contributed to unaccounted portion of the measure spectra, which is difficult to be evaluated in the simulation.

In TEXONO, the B_r spectral shape of $CR^+ \otimes AC^-$ (cosmic-induced events) is measured from n-type point-contact germanium detector with the assumption that surface events at low energy are negligible, which is unproven. These might produce significant unaccounted systematic uncertainties.

(2) **Normalization assumption.**

To obtain B_r of calibration sources, the spectra from simulations need to be normalized to the measured spectra at a certain energy range, where the values of ϵ_{BS} , λ_{BS} are assumed to be 1 [7, 9] in $\sim 2-4$ keV for various gamma sources and $CR^+ \otimes AC^-$. The assumption is unproven.

(3) **Singularity problem.**

The solutions of Eq. 2 are undefined when $\epsilon_{BS} + \lambda_{BS}$ approaches 1. This is avoidable if rise-time distributions are known.

In this report, we purpose an improved method to deal with bulk/surface separation without the spectral shape assumption and normalized assumption, thus avoid the systematic uncertainties associated with those assumptions.

3. B/S Selection: Ratio Method

3.1. Formulation

For any samples, e. g., calibration and background sources, the measured count rate at a certain energy-bin, E , and rise-time-bin, τ , could be expressed

as summation of the real bulk and surface count rate:

$$N_i(E, \tau) = N_{Bi}(E, \tau) + N_{Si}(E, \tau), \quad (4)$$

where i is the sources index, N_{Bi} and N_{Si} are the unknown rise-time distributions for bulk and surface events.

Assume those sources share a common bulk and surface rise-time distribution, then N_{Bi} and N_{Si} could be expressed as product of sources independent terms and τ independent terms:

$$\begin{aligned} N_{Bi}(E, \tau) &= B_i(E)f_B(E, \tau) \\ N_{Si}(E, \tau) &= S_i(E)f_S(E, \tau). \end{aligned} \quad (5)$$

Then, Eq. 4 could be rewritten as

$$N_i(E, \tau) = B_i(E)f_B(E, \tau) + S_i(E)f_S(E, \tau), \quad (6)$$

where f_B and f_S are sources independent rise-time distribution function for bulk and surface, B_i and S_i are τ independent scaling factors proportional to bulk and surface count rate.

Eq. 6 could not be solved unless extra constrain are provided, e. g., presumption of $f_B(E, \tau)$ and $f_S(E, \tau)$ in CoGeNT [19] or known $\int N_{Bi}(E, \tau)d\tau$ for certain sources in TEXONO or CDEX-1 [9, 6, 7].

In this report, we purpose that the ratio of bulk or surface count rates among different sources could serve as the required constrain (we name the new method as ratio method for this reason). From Eq. 5, it is obvious that the ratio of count rates are exactly the ratio of scaling factors among different sources:

$$\begin{aligned} N_{Bi}(E, \tau)/N_{Bj}(E, \tau) &= B_i(E)/B_j(E) \\ N_{Si}(E, \tau)/N_{Sj}(E, \tau) &= S_i(E)/S_j(E). \end{aligned} \quad (7)$$

Format of Eq. 6 reveals that absolute values of B_i and S_i are irrelevant, it is B_if_B and S_if_S that are relevant. We are free to choose the values of scaling factors, B_i and S_i , as long as they satisfy relations in Eq. 7.

Note that right hand side of Eq. 7 are τ independent, since all sources share a common rise-time distribution. This property allows us to present the scaling factors B_i , S_i as integration of $N_i(\tau)$ in the clean bulk or clean

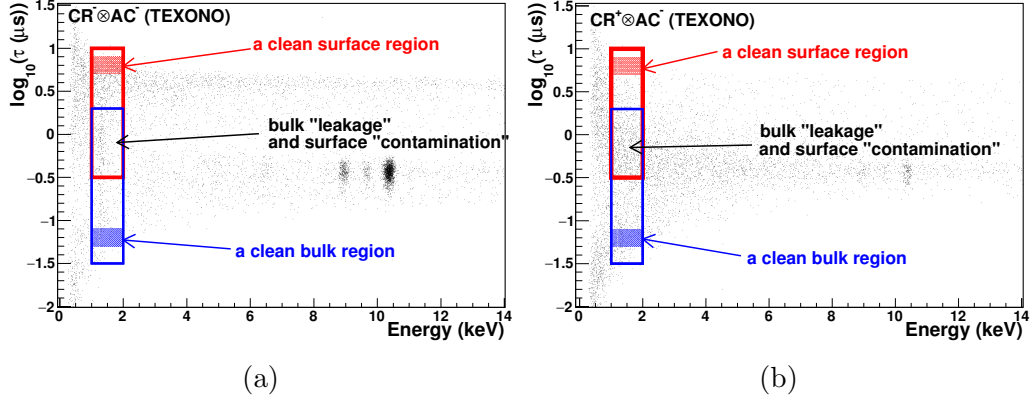


Figure 2: Rise-time vs. Energy for different sources (from TEXONO [8]): (a) anti-Compton vetoed and cosmic vetoed events, $\text{CR}^{-} \otimes \text{AC}^{-}$ and (b) cosmic-induced and anti-Compton vetoed events, $\text{CR}^{+} \otimes \text{AC}^{-}$. For a certain energy-bin (represent by boundaries of the blue or red boxes on x-axis), calculation of total bulk count and total surface count are complicated by bulk “leakage” or surface “contamination”. However, counts inside the “clean” regions free from “leakage” or “contamination” (represent as blue or red shadow boxes) should be proportional to total bulk or total surface counts, i. e., satisfy Eq. 7. This allows us to solve Eq. 9.

surface region (E has been dropped for convenient):

$$\begin{aligned} B_i &= \int_{b_0}^{b_1} N_{Bi}(\tau) d\tau \approx \int_{b_0}^{b_1} N_i(\tau) d\tau \\ S_i &= \int_{s_0}^{s_1} N_{Si}(\tau) d\tau \approx \int_{s_0}^{s_1} N_i(\tau) d\tau, \end{aligned} \quad (8)$$

as illustrated in Fig. 2, with $\tau \in (b_0, b_1)$ as boundaries of blue shadow box, and $\tau \in (s_0, s_1)$ as boundaries of red shadow box. The boundaries, b_0 , b_1 , s_0 and s_1 , could be arbitrary values, as long as they represent clean bulk or clean surface regions. The calculated scaling factors should satisfy Eq. 7.

In section 3.2, we will describe the procedure to correct the scaling factors, B_i and S_i , when b_0 , b_1 , s_0 and s_1 are not clean bulk and surface regions.

With the values of B_i and S_i being fixed, the solutions for f_{Bj} and f_{Sj} (binned version of $f_B(\tau)$ and $f_S(\tau)$, with j represents rise-time τ -bin) could be evaluated by minimize the χ^2 :

$$\chi_j^2 = \sum_i \frac{(B_i f_{Bj} + S_i f_{Sj} - N_{ij})^2}{\Delta N_{ij}^2}, \quad (9)$$

for each rise-time bin j , where N_{ij} is count rate of j^{th} rise-time bin and i^{th} -source.

We will interchange notations of $f_B(\tau)$, $f_S(\tau)$ and $N_i(\tau)$ with f_{Bj} , f_{Sj} and N_{ij} , although they are processed in numerical way. All the variables, B_i , S_i , $f_B(\tau)$, $f_S(\tau)$ and $N_i(\tau)$ are also function of energy, since each energy bin is treated independently, we omit the energy notation E in most of the equations.

The χ_j^2 in Eq. 9 sums over sources index, i , only. Solutions for each rise-time bin j , are independent of each other.

Note that, when there are only two sources (indexed as 0 and 1) involved, the solution for $B_0 f_B(\tau)$ is:

$$B_0 f_B(\tau) = \frac{N_1(\tau) - (S_1/S_0)N_0(\tau)}{B_1/B_0 - S_1/S_0}, \quad (10)$$

it is undetermined if $B_1/B_0 = S_1/S_0$, e. g., splitting a data set into two with each has the same rise-time distribution profile will not provide a solution. The solutions for $B_i f_B(\tau)$ and $S_i f_S(\tau)$ exist only if at least two of the sources satisfy $B_i/B_j \neq S_i/S_j$.

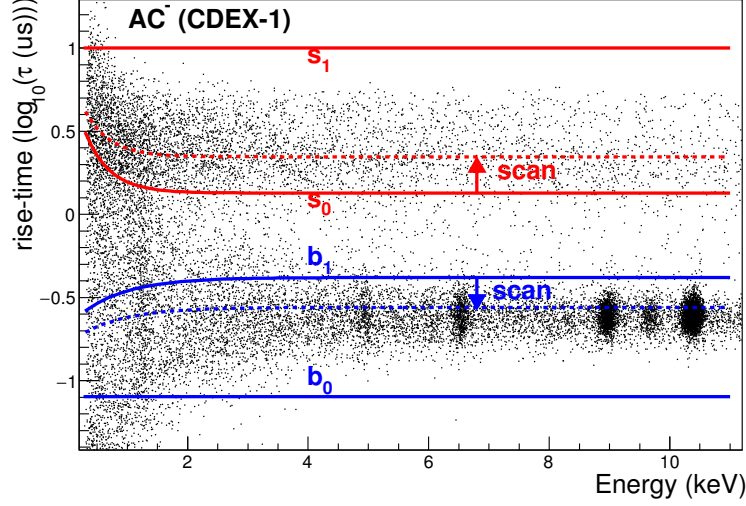


Figure 3: Rise-time vs. Energy, bulk and surface: choice of b_0 , b_1 , s_0 , s_1 . b_1 , s_0 will be scanned for systematic check.

3.2. Evaluation

Scaling factors in Eq. 8 are proportional to real bulk or surface count rates, N_{Bi} and N_{Si} , only if b_0 , b_1 , s_0 and s_1 in Eq. 8 represent clean regions of bulk and surface, which is not always the case.

As illustrate in Fig. 3, surface events leakage into b_0 , b_1 (or vice versa) is unavoidable.

Fortunately, B_i and S_i could be corrected by subtraction off the leakages evaluated from rise-time distributions of results of Eq. 9, perturbatively:

$$\begin{aligned} B_i &= B_i^0 - \int_{b_0}^{b_1} S_i^0 f_S(\tau) d\tau \\ S_i &= S_i^0 - \int_{s_0}^{s_1} B_i^0 f_B(\tau) d\tau, \end{aligned} \quad (11)$$

where f_B and f_S are solutions from minimizing Eq. 9. B_i^0 and S_i^0 are initial

scaling factors calculated from Eq. 8:

$$\begin{aligned} B_i^0 &= \int_{b_0}^{b_1} N_i(\tau) d\tau \\ S_i^0 &= \int_{s_0}^{s_1} N_i(\tau) d\tau, \end{aligned} \quad (12)$$

B_i and S_i are the scaling factors after correction.

The correction could be done in several iterations, until the scaling factors numerically converge:

$$\begin{aligned} B_i^{(n)} &= B_i^0 - \int_{b_0}^{b_1} S_i^{(n-1)} f_S^{(n-1)}(\tau) d\tau \\ S_i^{(n)} &= S_i^0 - \int_{s_0}^{s_1} B_i^{(n-1)} f_B^{(n-1)}(\tau) d\tau, \end{aligned} \quad (13)$$

where $f_B^{(n-1)}$ and $f_S^{(n-1)}$ are results of minimizing Eq. 9 at $(n-1)^{th}$ iteration.

Final real bulk and surface count rates for i^{th} source at energy bin E are calculated as:

$$\begin{aligned} B_{ri}(E) &= \int_{all \ \tau} N_{Bi}(E, \tau) d\tau = \int_{all \ \tau} B_i^{(n)}(E) f_B^{(n)}(E, \tau) d\tau, \\ S_{ri}(E) &= \int_{all \ \tau} N_{Si}(E, \tau) d\tau = \int_{all \ \tau} S_i^{(n)}(E) f_S^{(n)}(E, \tau) d\tau, \end{aligned} \quad (14)$$

For practical reason, we adopted 10 iterations for the results in this analysis, a 100 iterations version is used as systematic cross-check.

The B_i^0 and S_i^0 are calculated from unbinned data, while the $f_B(\tau)$ and $f_S(\tau)$ are binned functions. Integration $\int_{b_0}^{b_1} S_i^{n-1} f_S^{n-1}(\tau) d\tau$ is done in numerical way, when b_0 , b_1 , s_0 or s_1 do not fit the data binning, linear interpolation is used in the integration.

3.3. Uncertainties

There are three factors involved in final statistical errors:

1. Errors of f_B and f_S are calculated from $\chi_{min}^2 + 1$ of Eq. 9 for each τ -bin.
2. Errors of B_i^0 and S_i^0 .
3. Errors of correction term of $B_i^{(n-1)}$ and $S_i^{(n-1)}$ in Eq. 13.

Standard errors propagation are used to calculate statistical errors of B_{ri} and S_{ri} .

4. Data Analysis

Data from CDEX-1 [6, 7] has been re-analysed to demonstrate the ratio method, and compared with spectral shape method. Results from TEX-ONO [8, 9] will be used as a consistency check.

4.1. Best fit of rise-time distributions

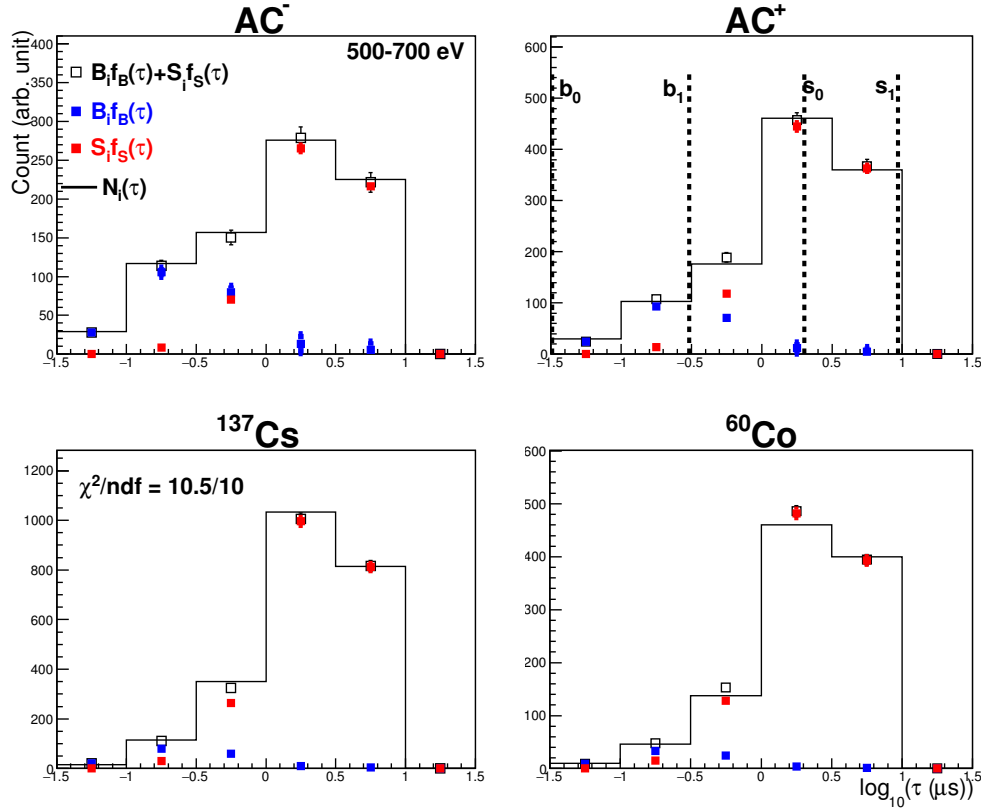


Figure 4: CDEX-1 : Best fit results for $f_B(\tau)$ and $f_S(\tau)$ at 500-700 eV, where $N_i(\tau)$ is the raw data, inputs to Eq. 9, and index $i = \{AC^-, AC^+, {}^{137}\text{Cs}, {}^{60}\text{Co}\}$.

In CDEX-1, two type of events are recorded in germanium detector, AC^- (dark matter candidate events) and AC^+ (mainly ambient gamma).

Four gamma sources, ${}^{241}\text{Am}$, ${}^{137}\text{Cs}$, ${}^{57}\text{Co}$ and ${}^{60}\text{Co}$, are used as calibration sources in the spectral shape method analysis. They are normalized to the

simulated background spectra shape. The spectral shape of AC^- and AC^+ are not known beforehand, they could not be used as calibration sources.

For ratio method, spectral shape assumption for calibration sources is not needed, AC^- and AC^+ could be used as calibration sources. Although AC^- and AC^+ are sufficient to solve Eq. 9, but both are slightly surface-rich at low energy (<1 keV), that will cause large uncertainties if both have similar bulk to surface ratio, due to small denominator effect described in Eq. 10.

In this analysis, we will use ^{137}Cs and ^{60}Co to compensate this effect. They have relatively smaller bulk to surface ratios, compared with AC^- and AC^+ , as shown in Fig. 4

^{241}Am and ^{57}Co are not used, although they show a similar rise-time profile as AC^- and AC^+ in low energy region (<1 keV), but not in high energy region (>2 keV).

Best fitted results for f_B and f_S at 500-700 eV are shown in Fig. 4.

4.2. Systematic uncertainties

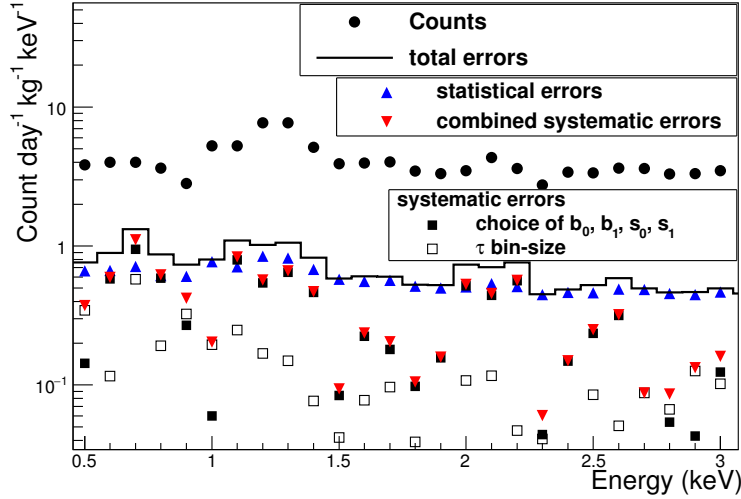


Figure 5: Errors budget: at low energy, the largest contribution comes from choice of b_0 , b_1 , s_0 and s_1 , while at higher energy errors are dominated by statistical errors. Note that first bin is 450-550 eV.

As shown in Fig. 5, the largest systematic uncertainties come from choice of b_0 , b_1 , s_0 and s_1 , we arbitrary shrink the range of (b_0, b_1) and (s_0, s_1)

according to Fig. 3 by 25%, and set the maximum different of count rate as related systematic errors.

The different from choice of b_0 , b_1 , s_0 and s_1 might well include part of statistic uncertainties of B_i and S_i , but, nevertheless we treat them as independent errors in this reports. 25% shrinking of b_1 or s_0 are chose to keep enough events for integrations of B_i^0 and S_i^0 .

The τ binning is also considered in this content. Different bin-size for B_i , S_i correction and bin-size for final f_B , f_S fitting are varied to assess the systematic uncertainties. Bin-size of 0.2, 0.4, 0.8 (in unit of $\log_{10}(\mu s)$) are set independently for both contents.

Systematic uncertainties from numbers of iterations of B_i , S_i corrections are negligible.

4.3. Goodness of fitting

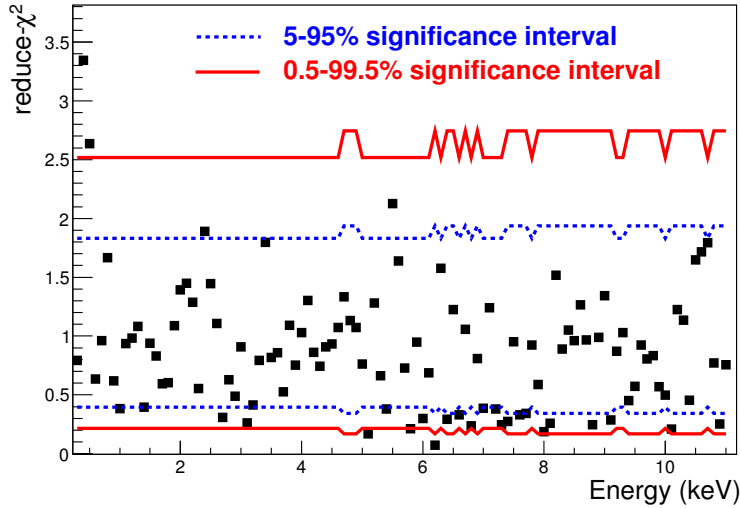


Figure 6: The reduced- χ^2 of each energy bin, along with related significant interval. First bin is 350-450 eV.

The reduced- χ^2 of each energy bin are shown in Fig. 6. Degree of freedoms of each energy are calculated as total numbers of non-zero τ -bins of all four sources subtract off total non-zero τ -bins of f_B and f_S . Significant intervals according to the degree of freedom are drawn on Fig. 6, it shows a reasonable

fitting results and justifies that all four calibration sources share similar rise-time profile above 350 eV.

4.4. AC^- spectrum and dark matter searches results

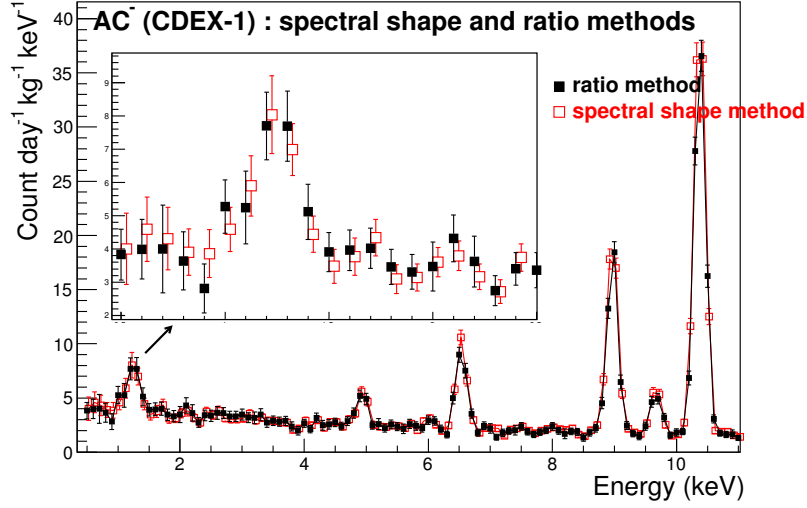


Figure 7: Comparing CDEX-1 [6, 7] spectra, spectral shape and ratio methods. Note that the threshold is 450 eV for ratio method and 475 eV for spectral shape method. Systematic errors are included.

The results of CDEX-1 are consistent between spectral shape and ratio methods, with ratio method slightly better in errors at low energy region, that is due to lack of bulk-rich sources for bulk/surface calibration in underground laboratory with spectral shape method [6, 7], which will contribute to larger uncertainty of ϵ_{BS} , while ratio method is less vulnerable to this problem, since AC^- itself could serve as bulk-rich source.

A comparison of AC^- spectrum and spin-independent exclusion plot of dark matter for spectral shape method and ratio method are shown in Fig. 7 and 8.

4.5. AC^+ , gamma and surface spectra

Beside a slower rise-time, another interested feature of surface events is incomplete energy deposition in the detector and the amount of energy

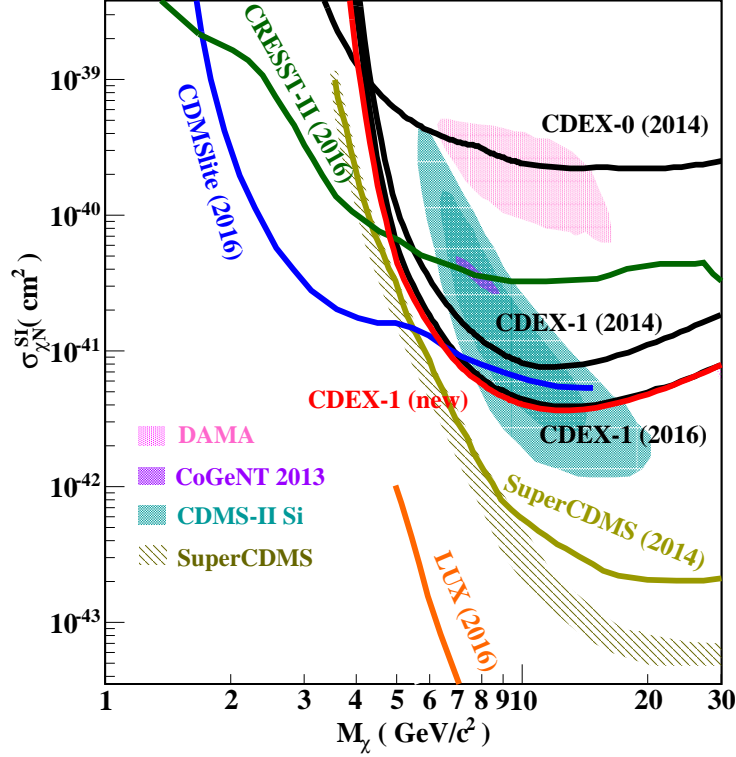
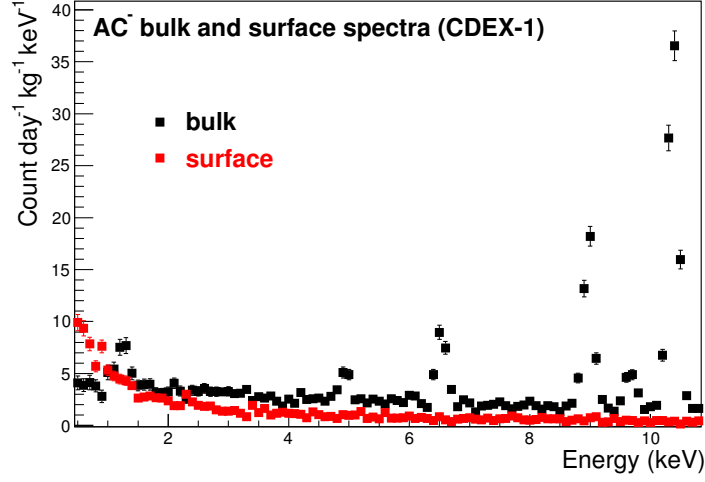
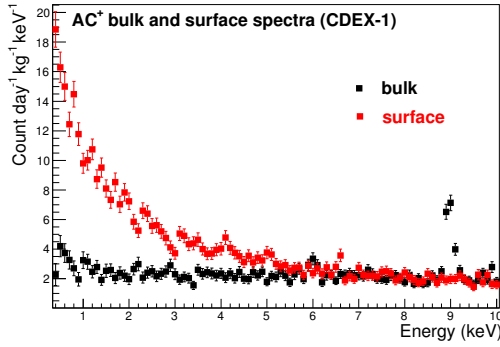


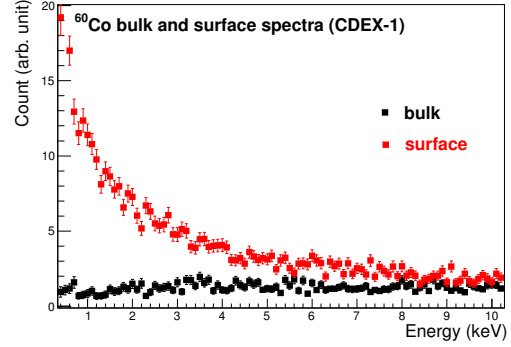
Figure 8: Comparing CDEX-1 [6, 7] spin-independent results, spectral shape method (denoted as CDEX-1(2016)) and ratio method (CDEX-1(new)). Also shown are 90% confidence upper limits from CDEX-0 (black curve) [22], CDEX-1 (black curve) [6], CDMSlite (blue curve) [23], CRESST-II (dark green curve) [24], SuperCDMS (olive curve) [25], and LUX (orange curve) [26], as well as detection claims from DAMA (pink region) [10, 12], CoGeNT (purple region) [14] and CDMS II Si (teal region) [16].



(a)



(b)



(c)

Figure 9: Bulk and surface spectra for (a) AC^- , (b) AC^+ and (c) ^{60}Co . All gamma peaks are correctly assigned to bulk's spectra, and all surface spectra are monotonic as expected.

deposited depends on location at dead layer, that will cause a continuous and monotonic energy spectrum with pile-up at low energy.

Indeed, Fig. 9 show that the surface spectra are monotonic and fit the description. The figures also show that all the gamma peaks have been correctly constructed as part of bulk spectra, this is not trivial, given that each energy bin are solved independently.

4.6. TEXONO data

Re-analyses of TEXONO [8] data also show consistent results.

Four types of events, $CR^- \otimes AC^-$, $CR^+ \otimes AC^-$, $CR^- \otimes AC^+$ and $CR^+ \otimes AC^+$ are recorded in germanium detector, with $CR^- \otimes AC^-$ being the dark matter candidate.

In the spectral shape method analysis of TEXONO data [8], ^{241}Am , ^{137}Cs and $CR^+ \otimes AC^-$ are used as B/S calibration sources. These three sources are then calibrated to the simulated spectral shape of ^{241}Am and ^{137}Cs , and $CR^+ \otimes AC^-$ measurement of n-type point-contact germanium detector.

In ratio method analysis, we use all four types of events, $CR^- \otimes AC^-$, $CR^+ \otimes AC^-$, $CR^- \otimes AC^+$ and $CR^+ \otimes AC^+$ as calibration sources, without using any gamma sources. As shown in Fig. 10, consistent results have been achieved.

The comparison shows that previous published results of TEXONO [8] and CDEX-1 [6, 7] are indeed on the right path.

5. Discussion

The ratio method provides an alternative way to deal with bulk/surface separation. It produces consistent results with spectral shape method (Fig. 7,10).

Both methods are based on the assumption that the bulk (and surface) rise-time distributions are similar between involved sources. In addition to this basis, the spectral shape assumption and normalization assumption are needed in the spectral shape method analysis. While in the ratio method, we assume that bulk (and surface) ratios between different sources are known.

The most promising advantage of the ratio method is that the calibration is done with in situ data, e. g., dark matter candidate data, as well as cosmic-induced or ambient gamma-induced data. Those samples are slightly bulk-rich, thus compensate the lacking of bulk-rich calibration sources at underground laboratories, where bulk-rich cosmic-induced events are hard to come by. This property also reduces the necessity of various gamma sources

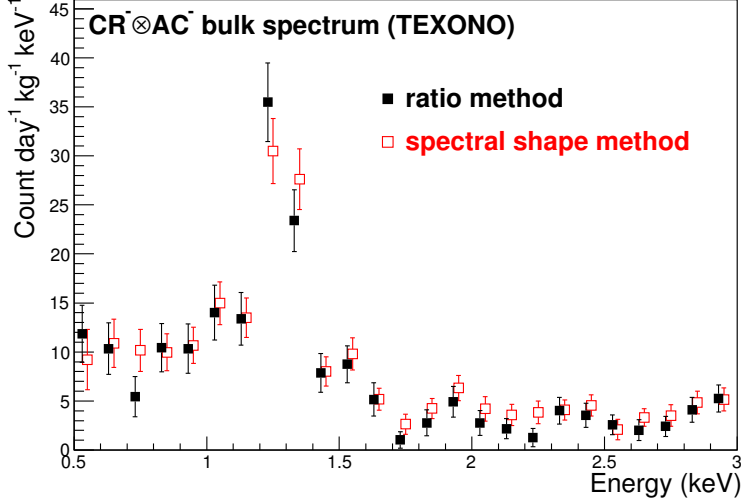


Figure 10: Comparing TEXONO [8] results, spectral shape and ratio methods. Note that the values of x-axis have been shifted for more presentable.

for calibration and allows long term stability assessment, where using gamma sources will be unpractical.

However, there are shortcomings with the ratio method, it need sufficient counts for 2D-binning (E and τ). Since f_B and f_S are positive definite, solutions of f_B (f_S) at regions of τ which supposed to be $f_B = 0$ ($f_S = 0$) will bias toward positive results due to statistic fluctuation around zero, if τ bin-size is too small. This limits the choice for larger bin-size in this analysis.

6. Acknowledgment

This work is supported by the Academia Sinica Investigator Award 2011-15, contracts 103-2112-M-001-024 and 104-2112-M-001-038-MY3 from the Ministry of Science and Technology of Taiwan and the National Natural Science Foundation of China (Nos.11175099, 11275107, 11475117, 11475099 and 11475092) and the National Basic Research Program of China (973 Program) (2010CB833006) and the Tsinghua University Initiative Scientific Research Program No.20121088494.

References

References

- [1] Q. Yue, et al., Detection of WIMPs using low threshold HPGe detector, *High Energy Phys. Nucl. Phys.* 28 (2004) 877.
- [2] H. T. Wong, et al., Research program towards observation of neutrino-nucleus coherent scattering, *J. Phys. Conf. Ser.* 39 (2006) 266.
- [3] A. K. Soma, et al., Characterization and performance of germanium detectors with sub-keV sensitivities for neutrino and dark matter experiments, *Nucl. Instr. Meth. Phys. Res. A* 836 (2016) 67–82.
- [4] P. N. Luke, et al., Low capacitance large volume shaped-field germanium detector, *IEEE Trans. Nucl. Sci.* 36 (1989) 926.
- [5] W. Zhao, et al., First results on low-mass WIMPs from the CDEX-1 experiment at the China Jinping Underground Laboratory, *Phys. Rev. D* 88 (2013) 052004.
- [6] Q. Yue, et al., Limits on light weakly interacting massive particles from the CDEX-1 experiment with a p-type point-contact germanium detector at the China Jinping Underground Laboratory, *Phys. Rev. D* 90 (2014) 091701(R).
- [7] W. Zhao, et al., Search of low-mass WIMPs with a p-type point contact germanium detector in the CDEX-1 experiment, *Phys. Rev. D* 93 (2016) 092003.
- [8] H. B. Li, et al., Limits on spin-independent couplings of WIMP dark matter with a p-type point-contact germanium detector, *Phys. Rev. Lett.* 110 (2013) 261301.
- [9] H. B. Li, et al., Differentiation of bulk and surface events in p-type point-contact germanium detectors for light WIMP searches, *Astropart. Phys.* 56 (2014) 1–8.
- [10] P. Belli, et al., Observations of annual modulation in direct detection of relic particles and light neutralinos, *Phys. Rev. D* 84 (2011) 055014.

- [11] R. Bernabei, et al., First results from DAMA/LIBRA and the combined results with DAMA/NaI, *Eur. Phys. J. C* 56 (2008) 333.
- [12] R. Bernabei, et al., New results from DAMA/LIBRA, *Eur. Phys. J. C* 67 (2010) 39.
- [13] C. E. Aalseth, et al., Results from a search for light-mass dark matter with a p-type point contact germanium detector, *Phys. Rev. Lett.* 106 (2011) 131301.
- [14] C. E. Aalseth, et al., CoGeNT: A search for low-mass dark matter using p-type point contact germanium detectors, *Phys. Rev. D* 88 (2013) 012002.
- [15] C. E. Aalseth, et al., Search for an annual modulation in three years of CoGeNT dark matter detector data, 2014. [ArXiv:1401.3295](#).
- [16] R. Agnese, et al., Silicon detector dark matter results from the final exposure of CDMS II, *Phys. Rev. Lett.* 111 (2013) 251301.
- [17] R. D. Martin, et al., Determining the drift time of charge carriers in p-type point-contact HPGe detectors, *Nucl. Instr. Meth. Phys. Res. A* 678 (2012) 98–104.
- [18] E. Aguayo, et al., Characteristics of signals originating near the lithium-diffused N+ contact of high purity germanium p-type point contact detectors, *Nucl. Instr. Meth. Phys. Res. A* 701 (2013) 176 – 185.
- [19] C. E. Aalseth, et al., Maximum likelihood signal extraction method applied to 3.4 years of CoGeNT data, 2015. [ArXiv:1401.6234v3](#).
- [20] H. Jiang, et al., Measurement of the dead layer thickness in a p-type point contact germanium detector, *Chin. Phys. C* 40 (2016) 096001.
- [21] J. L. Ma, et al., The study of dead layer characteristics of a p-type point contact germanium detector, *Appl. Radiat. Isot.* (in press).
- [22] S. K. Liu, et al., Limits on light WIMPs with a germanium detector at 177 eVee threshold at the China Jinping Underground Laboratory, *Phys. Rev. D* 90 (2014) 032003.

- [23] R. Agnese, et al., New results from the search for low-mass weakly interacting massive particles with the CDMS low ionization threshold experiment, *Phys. Rev. Lett.* 116 (2016) 071301.
- [24] G. Angloher, et al., Results on light dark matter particles with a low-threshold CRESST-II detector, *Eur. Phys. J. C* 76 (2016) 25.
- [25] R. Agnese, et al., Search for low-mass weakly interacting massive particles with SuperCDMS, *Phys. Rev. Lett.* 112 (2014) 241302.
- [26] D. S. Akerib, et al., Results from a search for dark matter in the complete LUX exposure, 2016. [ArXiv:1608.07648v2](https://arxiv.org/abs/1608.07648v2).